

Blue laser welding of low thickness Ni-coated copper and mild steel for electric vehicle (EV) battery manufacturing

Sadeghian, A & Iqbal, N

Published PDF deposited in Coventry University's Repository

Original citation:

Sadeghian, A & Iqbal, N 2022, 'Blue laser welding of low thickness Ni-coated copper and mild steel for electric vehicle (EV) battery manufacturing', *Optics and Laser Technology*, vol. 155, 108415

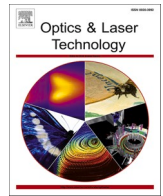
<https://dx.doi.org/10.1016/j.optlastec.2022.108415>

DOI 10.1016/j.optlastec.2022.108415

ISSN 0030-3992

Publisher: Elsevier

This is an Open Access article distributed under the terms of the Creative Commons Attribution License (<http://creativecommons.org/licenses/by/4.0/>), which permits unrestricted use, distribution, and reproduction in any medium, provided the original work is properly cited..



Full length article

Blue laser welding of low thickness Ni-coated copper and mild steel for electric vehicle (EV) battery manufacturing

Amirhossein Sadeghian^{a,*}, Naveed Iqbal^{a,b}^a Institute for Advanced Manufacturing and Engineering, Coventry University, CV6 5LZ, UK^b ITP Aero, Dorey Way, Hucknall, Nottinghamshire NG15 6EU, UK

ARTICLE INFO

Keywords:

Blue laser welding
Electric vehicle battery
Copper
Mild steel
Microstructure
Joint strength

ABSTRACT

Modern advancements in blue lasers offer a promising alternative to conventional infrared laser welding of highly-reflective battery materials. In this study, a high-power blue laser system was used to weld the low thickness Ni-coated copper and mild steel used in 18650-type cylindrical cells. The effect of laser power on the penetration depth, interface width, and weld bead quality was studied. The weld microstructure was characterized by employing optical microscopy, scanning electron microscopy, and energy-dispersive X-ray spectroscopy. The mechanical performance of the welds was evaluated through peel testing and microhardness measurements. The results show that the penetration depth and weld width increased with laser power. Increasing the laser power to more than 1.3 kW resulted in a damaging effect on weld bead quality creating defects such as crack, under-fill, and distortion due to excessive heat input. Weld samples fractured in the heat-affected zone of Ni-coated copper during peel testing due to grain growth in copper. The maximum peel strength of 158.8 N was achieved for the 1.2 kW sample. The formation of a composite microstructure between Cu and Fe with a higher hardness than parent metals was observed inside the weld nugget. The hardness of this zone increased with the laser power due to an increase in the amount of Fe, reaching 185 HK for the 1.5 kW sample. By exposure to a corrosive environment, the peel strength drastically decreased and the failure occurred at the weld interface. For the 1.2 kW sample, the peel strength was reduced to around 57 N. The process initially developed for coupons of Ni-coated copper and mild steel was further tested on the positive and negative tabs of 18650-type cylindrical cells. The weld microstructure showed a lack of defects. However, due to varying thicknesses and associated heat sinks further process refinement is required for optimum joint quality.

1. Introduction

Due to fossil fuel consumption, transportation is currently responsible for a considerable amount of global CO₂ emissions, significantly higher than the targets set by the climate change policies [1]. This situation has prompted the rapid development of electric vehicles (EVs) in order to drastically reduce the greenhouse gases released by the transport sector [2,3]. EVs usually operate with electricity stored in lithium-ion (Li-ion) batteries owing to their advantages with one of the main advantages being the high energy density [4]. A typical Li-ion EV battery system consists of several hundred up to thousands of single battery cells joined together to provide the required energy [5]. Each of these joints directly influences the battery's durability, functional reliability, and overall vehicle performance [6]. This makes the production of quality joints with good mechanical strength and high electrical conductivity an

issue of critical importance [7–9].

Laser welding is an attractive process for joining cells in EV battery manufacturing owing to its non-contact nature, high efficiency, narrow heat-affected zone (HAZ), and high quality of welds [10–14]. However, the low absorptivity of the materials used in EV batteries such as copper, aluminum, and nickel often undermines the welding efficiency and leads to unstable weld quality in conventional industrial laser welding with the infrared wavelength (~1064 nm) [15]. One way to overcome this challenge is to use novel laser beams with better absorptivity such as newly-developed blue or green laser systems [16,17]. The industrial application of these lasers has been limited until recently due to their low peak power. However, new advances have significantly increased the output power, up to around 1.5 kW, thereby providing new opportunities for novel applications such as laser welding [18,19]. It has been shown that the absorptivity value of the blue laser (wavelength: ~ 450

* Corresponding author.

E-mail address: sadeghiana@uni.coventry.ac.uk (A. Sadeghian).<https://doi.org/10.1016/j.optlastec.2022.108415>

Received 16 February 2022; Received in revised form 23 May 2022; Accepted 24 June 2022

Available online 9 July 2022

0030-3992/© 2022 The Authors. Published by Elsevier Ltd. This is an open access article under the CC BY license (<http://creativecommons.org/licenses/by/4.0/>).

Table 1
The chemical composition of materials used for blue laser welding (wt %).

	Cu	Fe	C	Mn	P	S	Pb	Bi
C103 copper	Bal.	–	–	–	<0.007	–	<0.005	<0.001
DC01 steel	–	Bal.	<0.12	<0.6	<0.045	<0.045	–	–

nm) at room temperature for various metals is several times higher than the infrared laser [20]. For example, copper, aluminum, and nickel have respectively 13, 3, and 1.5 times higher absorptivity for blue wavelength [21]. This can potentially result in a more stable weld pool during the laser welding with less spatter, porosity and defects thereby enhancing the weld quality in difficult-to-weld high-reflective metals [22].

There is limited information in the public domain on the application of blue laser welding especially for joining dissimilar materials. Zediker *et al.* [23] reported an excellent weld quality without spatter or porosities for bead-on-plate blue laser welding of copper, stainless steel, and aluminum. Morimoto *et al.* [24] investigated the bead-on-plate welding of 200 μm thickness pure copper using the blue laser and reported full penetration at the laser intensity of $1 \times 10^7 \text{ W/cm}^2$ with a spot diameter of 50 μm . Das *et al.* [25] utilized a blue laser system to join 20 layers of low thickness (25 μm) foils to a single foil (200 μm) made of AISI 316L stainless steel. They stated that the weld geometry and the joint strength were greatly influenced by the blue laser which reduced the discontinuities in the weld region. The effect of beam wavelength in the laser welding of CuSn₆ and Cu-ETP butt and overlap joints was studied by Hummel *et al.* [26]. It was reported that the beam absorptivity during the welding process was increased by decreasing the laser wavelength from 1070 nm to 515 nm and then to 450 nm. With the right parameters, the penetration depths of 648 μm for CuSn₆ and 312 μm for Cu-ETP were achieved in micro-welding with the blue laser.

At the moment, a stable joining process for highly-reflective battery materials is of great importance to the EV manufacturing industry. This paper reports the findings on the application of a blue laser system for joining low thickness Ni-coated copper and mild steel. The optimum process parameters (i.e., laser power, welding speed, etc.) to achieve good quality welds based on higher mechanical strength and sound microstructure are reported. Furthermore, the effect of a corrosive environment on joint strength and mode of failure has been studied. Based on the coupon welding, the blue laser is used for the first time to

weld positive and negative tabs of 18650-type cylindrical cells. These results provide new insights into the blue laser welding of low-thickness dissimilar materials for producing EV battery packs.

2. Materials and methods

The materials used in this study included high-purity Ni-coated copper (C103) and Ni-coated mild steel (DC01). The chemical compositions of materials are given in Table 1. Two sets of samples were produced to investigate the applicability of the blue laser welding process for coupons and cylindrical cells. The first set of samples included coupon welding of 0.3 mm thick Ni-coated Cu and 0.6 mm thick Ni-coated mild steel sheets. The dimension of the sheets was 140 mm \times 100 mm. The Ni coating with a thickness of 3 μm was electrodeposited on both sides of sheets prior to welding to improve the corrosion resistance and weldability. The second set of samples involved welding Ni-coated Cu to positive and negative terminals of 18650-type cylindrical cells made of Ni-coated mild steel. The thickness of the Ni-coated Cu was 0.3 mm. The thickness of the positive terminal was 0.6 mm and the negative terminal had a thickness of 0.3 mm.

The laser welding was performed in a linear pattern using a continuous wave (CW) blue laser (LDMblue 1500–60, laserline, Germany), with a maximum peak power of 1.5 kW and a wavelength of 450 nm. The overlap joint configuration was used for all samples with the Ni-coated Cu on the top. Before welding, all samples were degreased with acetone to remove any surface contamination. A manual localized clamping on overlapping thin sheets was applied during welding to make sure there was no gap between sheets at the weld locations. During welding, the coupon samples were mounted on a thick stainless steel backing plate. High purity argon (99.99%) was selected as the shielding gas. Fig. 1 shows the laser welding setup used in this study.

Initially, a number of trial experiments were carried out to attain a visually acceptable weld appearance. Based on these trials, the laser

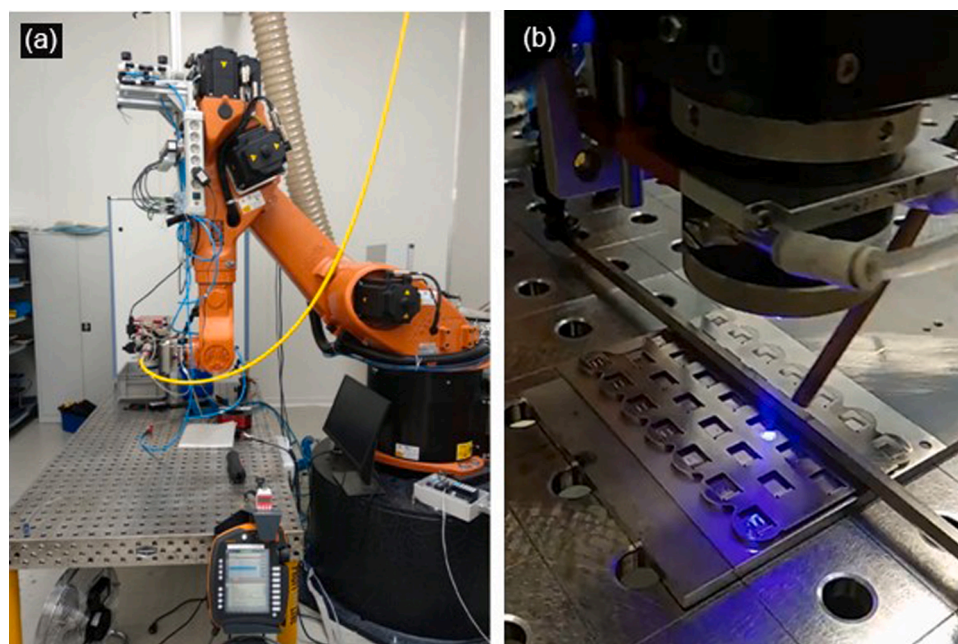


Fig. 1. (a) The robotic blue laser welding setup (b) laser welding head.

Table 2
Laser welding process parameters for blue laser welding.

Welding parameters	Value/type
Laser Power (kW)	Coupon: 1.1, 1.2, 1.3, 1.4, 1.5 Cylindrical cell: 1.3, 1.4, 1.5
Welding speed (m/min)	3, 3.5, 4, 4.5, 5, 5.5, 6
Shielding gas	Argon
Shielding gas flow rate (L/min)	5, 10, 15
Beam diameter (μm)	600
Focal position	At the surface

beam size was selected to be 600 μm, the focal position was set at the surface, the shielding gas flow 5 L/min, and the welding speed was chosen as 6 m/min. Laser power was chosen as the experimental variable. For coupon welding, the laser power was varied from 1.1 kW to 1.5 kW by the steps of 0.1 kW. After coupon welding, the process was repeated to weld negative and positive terminals of the 18650-type cylindrical cells using laser powers of 1.3 kW, 1.4 kW, and 1.5 kW. Other welding parameters were identical to the coupon welding. The laser process parameters used in this study are listed in Table 2.

For subsequent metallographic investigations, the weld samples were cut in the middle of the weld perpendicular to the weld line with an EDM machine and then were resin-mounted. The specimens were ground using 120 to 1200-grade SiC paper and were subsequently

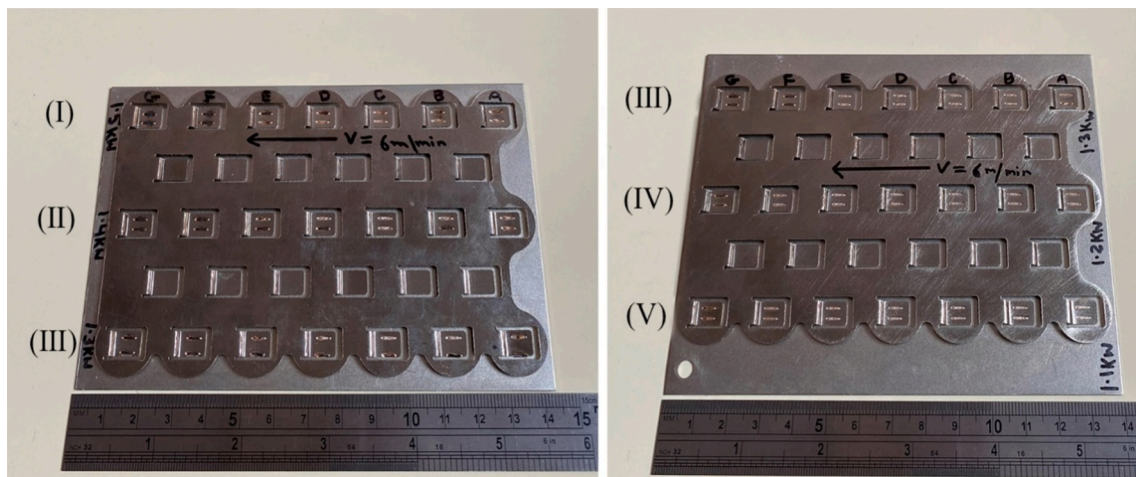


Fig. 2. The outlook of coupon samples, Ni-coated Cu on top and Ni-coated mild steel at the bottom produced using a constant welding speed of 6 m/min and varying laser powers of (I) 1.5 kW (II) 1.4 kW (III) 1.3 kW (IV) 1.2 kW (V) 1.1 kW.

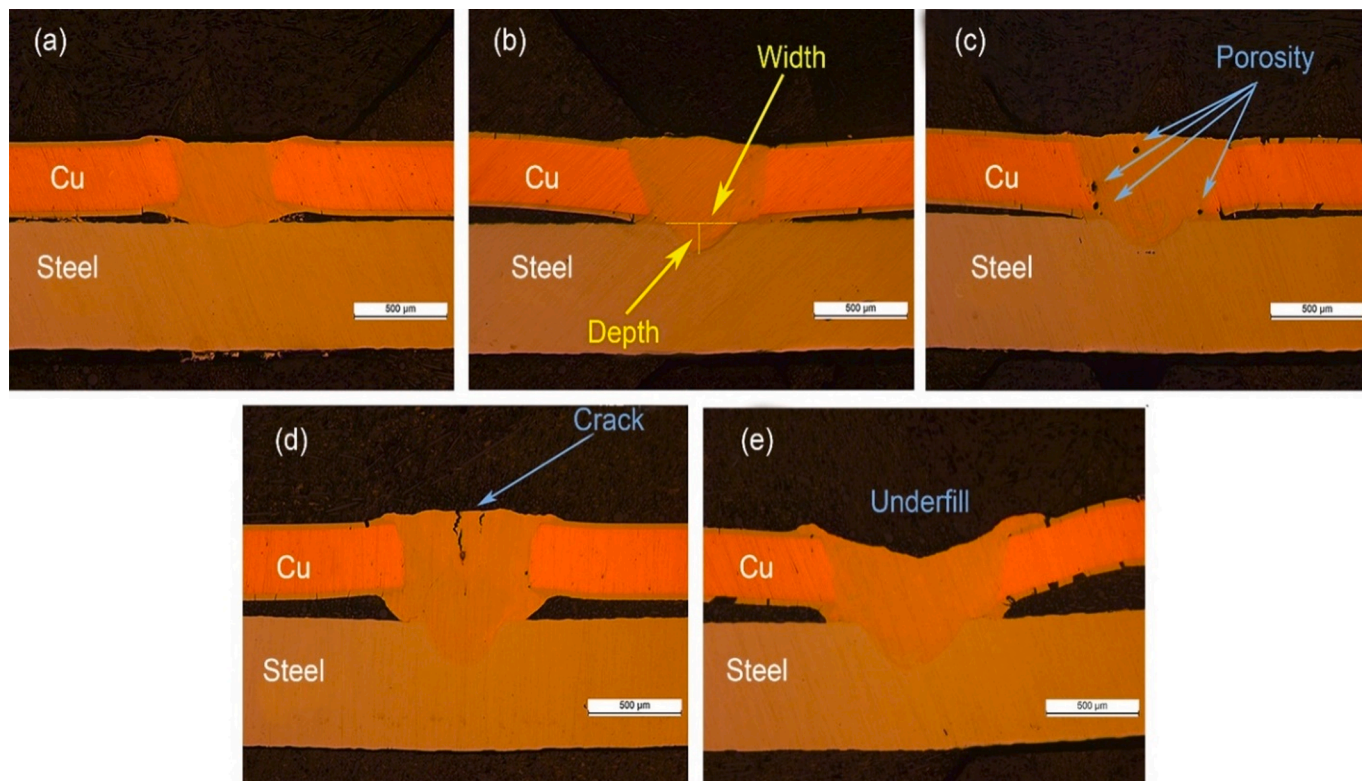


Fig. 3. The cross-sectional view of coupon weld samples with laser powers of (a) 1.1 kW (b) 1.2 kW (c) 1.3 kW (d) 1.4 kW (e) 1.5 kW.

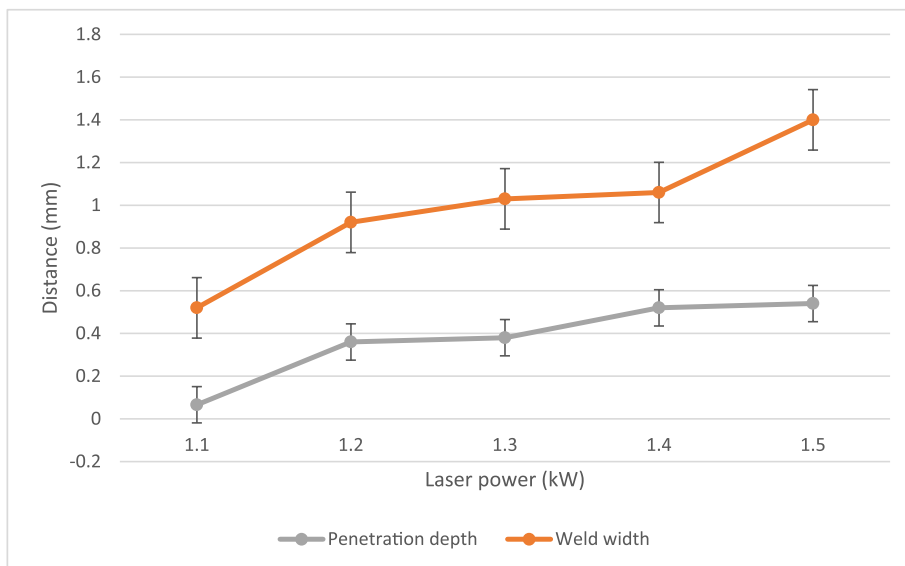


Fig. 4. The effect of laser power on the weld width and the depth of penetration.

polished using 9 μm, 3 μm, and 1 μm diamond suspension solutions. The weld microstructure was analyzed using a Leica DFC295 optical microscope and a Hitachi TM4000 tabletop scanning electron microscope (SEM) equipped with energy-dispersive X-ray spectroscopy (EDX). The weld strength was evaluated through peel testing which was performed using Nordson DAGE 4000Plus machine. Furthermore, Knoop microhardness was measured in different microstructural zones using a test load of 100 gf. To study corrosion behavior, the coupon weld samples were exposed to cyclic corrosion testing using Ascott CC1000ip test chamber with 5 vol% NaCl solution for 144 h at a temperature of 46 °C. These samples afterwards were subjected to peel testing for a comparative study of the mechanical performance of laser welded samples

before and after being exposed to a corrosive environment.

3. Results and discussion

3.1. Coupon welding

The experimental trials were conducted to identify the suitable process parameters window for fast and reliable welding. Shielding gas flow rates of 10 L/min and 15 L/min resulted in no joint due to heat being carried away as a result of the high flow of gas on the work surface. Thus, a flow rate of 5 L/min was selected. In trial experiments, welding speeds of 3 m/min, 3.5 m/min, 4 m/min, 4.5 m/min, 5 m/min, 5.5 m/

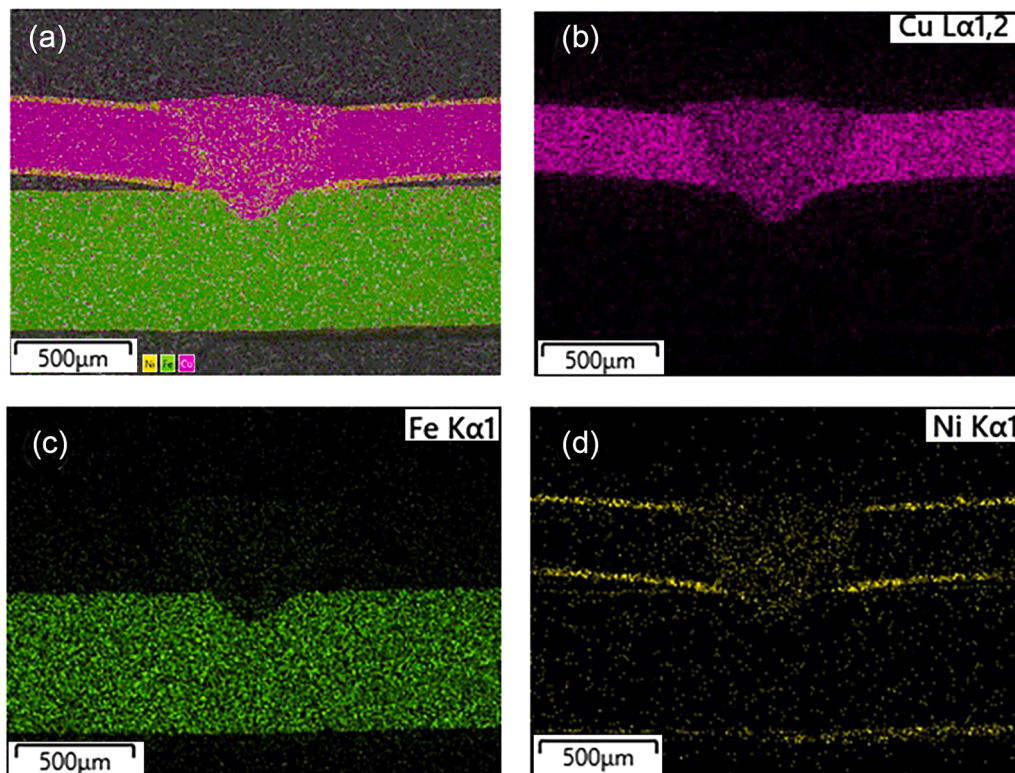


Fig. 5. The EDX map showing elemental distribution for the sample with a laser power of 1.2 kW (a) all elements (b) Cu (c) Fe (d) Ni.



Fig. 6. The EDX line scan inside the weld nugget (see insert) for the sample with a laser power of 1.2 kW.

min and 6 m/min were tested. From the visual inspection of the backside of the welded samples, overpenetration was observed for welding speeds lower than 6 m/min. Furthermore, selecting a high welding speed was considered more beneficial to the manufacturing industry due to the need for higher production rates. Thus, the welding speed was set to 6 m/min and welding power was considered the variable for further investigation. The top view of coupon samples, with double weld line geometry and a varying power from 1.1 kW to 1.5 kW is shown in Fig. 2. The visual inspection generally revealed weld beads with smooth surfaces for the laser powers of 1.1 kW, 1.2 kW, and 1.3 kW. However, increasing laser power to 1.4 kW and 1.5 kW gave rise to a detrimental

effect on the weld bead quality by creating discontinuities and surface concavity owing to the excessive heat input.

The optical micrograph of the weld cross-section for each laser power is shown in Fig. 3. The results indicate the increase in welding depth and width thereby creating a larger size melt pool with increasing laser power. For laser power of 1.1 kW, there was just enough heat input to melt the Ni-coated copper with a slight penetration into the bottom sheet, categorized as “under-weld” condition. For higher laser powers of 1.4 kW and 1.5 kW, the weld samples showed defects such as cracking and under-fill. Furthermore, the increase in welding distortion can be observed in samples with higher welding powers, especially in the 1.5

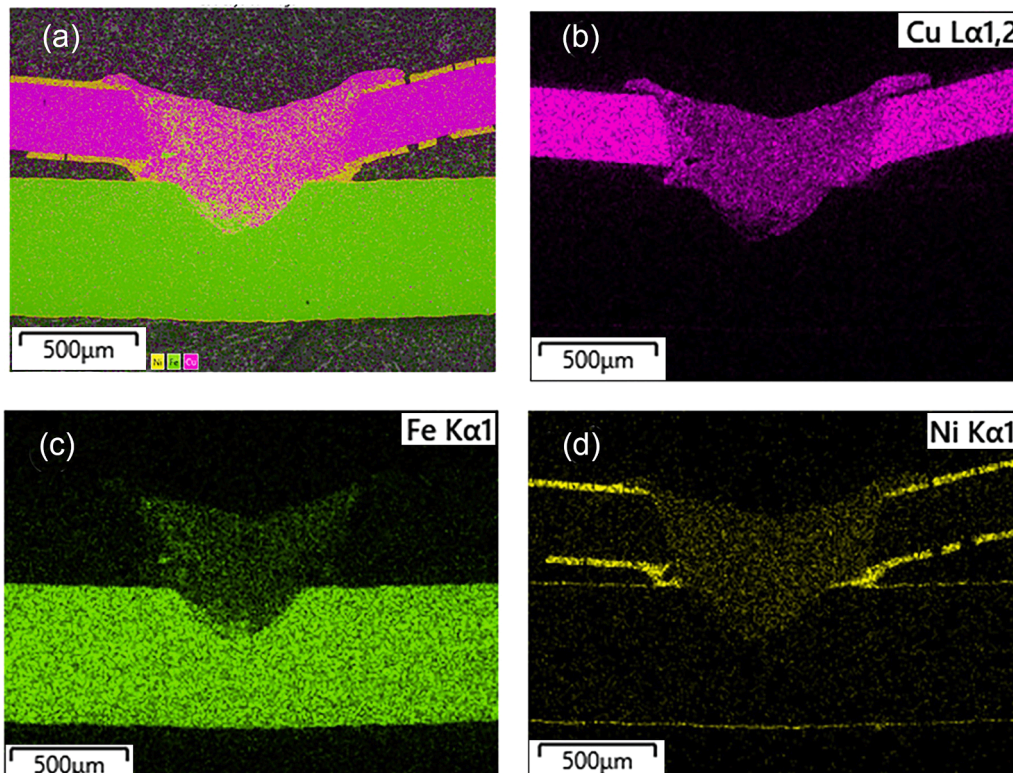


Fig. 7. The EDX map showing elemental distribution for the sample with a laser power of 1.5 kW (a) all elements (b) Cu (c) Fe (d) Ni.

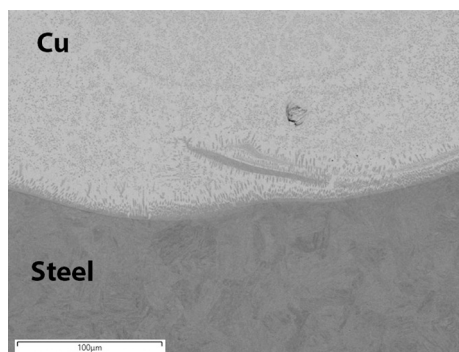


Fig. 8. The high-magnification SEM image of Cu and mild steel interface in the 1.5 kW sample showing an island-like structure of Fe-rich zones inside the Cu matrix.

kW sample. The crack formation can be attributed to the higher specific heat, causing larger temperature gradients, and producing higher residual stresses in the weld region which results in the appearance of cracks inside the weld nugget. In addition, the intermixing of Cu and Fe inside the weld nugget which is expected to increase with higher heat input can cause cracking during cooling due to phase separation and the difference in solidification rates [28]. The formation of under-fill which is a complex phenomenon has been attributed to the high weld pool turbulence in the samples with high heat input by researchers such as Pakmanesh et al. [27] who have thoroughly investigated the under-fill formation during the laser welding of thin sheets. Another interesting observation is the presence of minor porosities which can be seen inside the weld nugget of the 1.3 kW sample. Porosity is a common phenomenon in laser welding and is a result of a combination of a number of factors including the collapse of the keyhole and weld pool flow dynamic [28]. It has been found that porosity formation is strongly linked to the depth-to-width aspect ratio of the welds.

The larger the depth-to-width ratio, the easier porosity can form [29]. In other words, if the weld zone is shallow, less time is needed for a pore to move towards the surface and the number of pores will be

reduced. The effect of laser power on the weld width and the depth of penetration is shown in Fig. 4. The weld width was measured at the interface between the two sheets, while the penetration depth into the lower sheet was measured from the interface between the two materials (Fig. 3 b). Both the weld width and penetration depth increased with laser power due to the increasing heat input creating a bigger weld pool. Moreover, the results indicate that the weld width was always higher than the penetration depth, a typical characteristic of conduction mode laser welding. As can be deduced from Fig. 4, in the 1.3 kW sample, porosities were formed due to a relatively high ratio of depth to width. However, the number and size of these pores are small and negligible and are unlikely to affect the mechanical properties of joints. Overall, the 1.2 kW and 1.3 kW samples exhibited better weld microstructure with moderate weld penetration, no crack formation, or under-fill present.

Extremely high temperature inside the melt pool and the subsequent fast cooling during laser welding trigger thermal gradients causing diffusion and intermixing of weld metals. Fig. 5 exhibits the EDX mapping of the 1.2 kW sample illustrating intermixing of Ni, Cu, and Fe elements inside the weld nugget. Due to relatively low heat input fluid flow was not high and little Fe melted and mixed into the weld pool. Cu and Ni are normally soluble in solid-state and do not form any intermetallic compounds or cause cracking due to fragile products [30]. Nickel is chosen as the coating material owing to its good solubility in both Cu and Fe without producing brittle intermetallic phases [31,32]. However, Cu and Fe are immiscible in solid-state and produce an inhomogeneous solution. The EDX line scan illustrating the elemental distribution along the weld penetration in the 1.2 kW sample is shown in Fig. 6. The results indicated that the amount of Ni is relatively higher in molten Cu compared to that observed in molten steel. Ni coating on Cu and mild steel appeared to have melted and dissolved predominantly in the molten Cu. Fe and Cu concentrations fluctuated slightly inside the weld nugget illustrating an inhomogeneous distribution of these elements. The laser weld produced with higher laser power of 1.5 kW, exhibit more inhomogeneous elemental distribution as shown in Fig. 7. While the molten Fe is spread inside the molten Cu, there were local regions with higher amounts of Fe and a strong heterogeneity of the

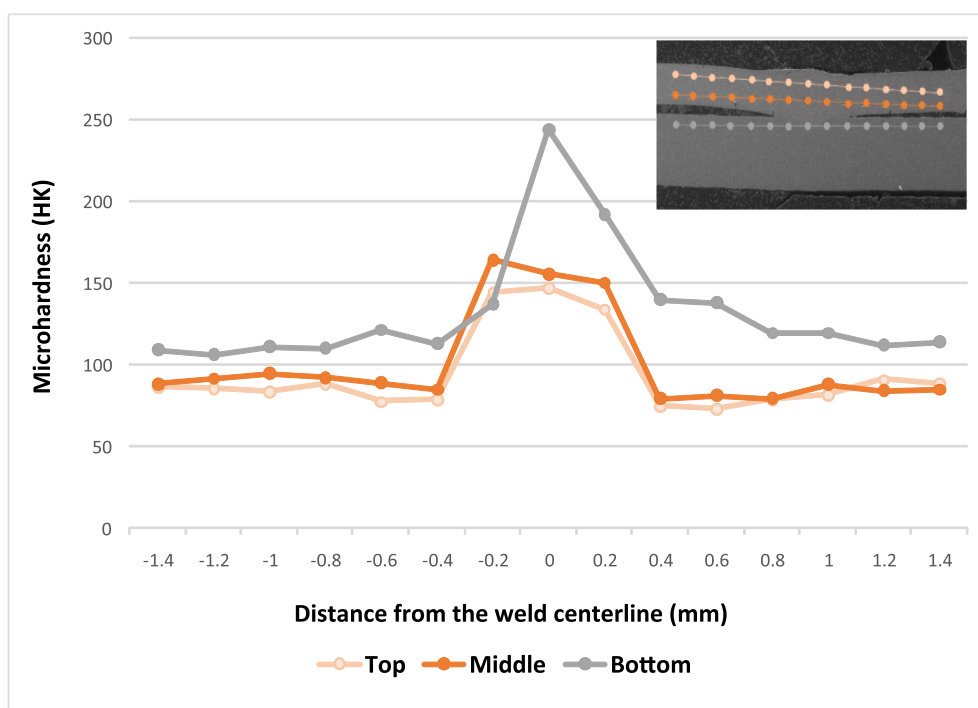


Fig. 9. Microhardness variation for the 1.2 kW sample, three horizontal line scans (see insert) across the weld nugget.

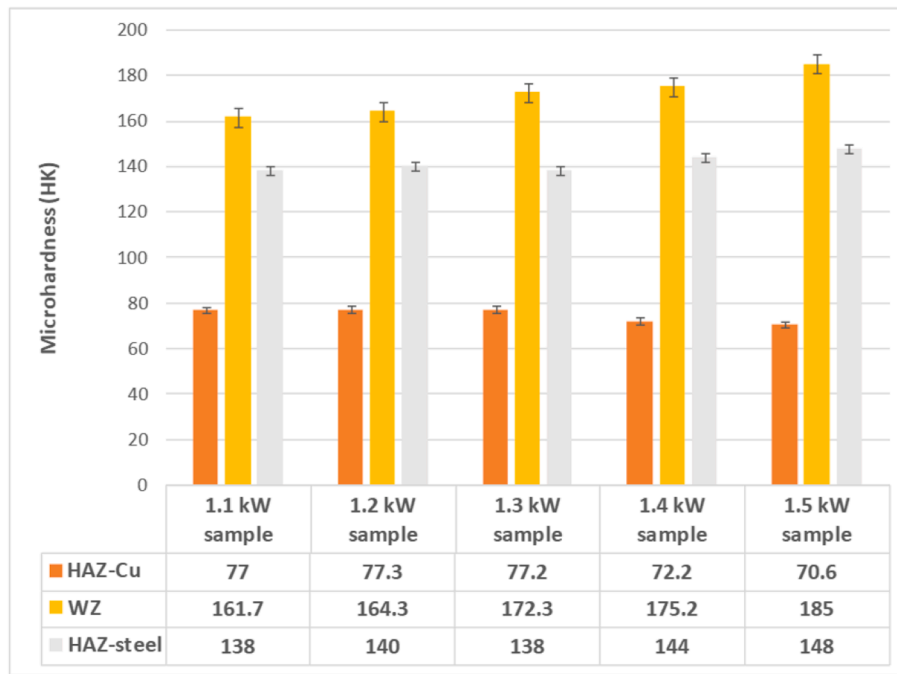


Fig. 10. The variation in average microhardness of weld nugget, HAZ of Cu, and HAZ of mild steel.

distribution of the main elements inside the weld nugget.

By comparing Fig. 5 and Fig. 7 it can be concluded that the Fe content in the weld zone increased with the increase of heat input due to higher penetration depth into the bottom sheet. Furthermore, at higher weld depths, the effects of increasing phase separation between both metals can be seen in the formation of widely spread small islands of high Fe concentration in the Cu-dominated matrix. Fig. 8 shows the high-magnification SEM image of the interface between Cu and mild steel in the 1.5 kW sample. The inhomogeneity of microstructure and island-like presence of Fe-rich zones inside the Cu matrix can be observed.

The horizontal line scans for microhardness variation across the weld nugget of the 1.2 kW sample are shown in Fig. 9. The results indicate a significant difference in the microhardness of the weld nugget compared to parent materials. The highest value of the hardness inside the weld nugget was about 250 HK, much higher than the hardness in the copper or mild steel, which were measured to be about 88 HK and 120 HK, respectively. This increased hardness inside the weld nugget can be attributed to the inter-mixing of Cu and Fe elements producing a composite microstructure. Such Fe-Cu composite microstructure has been reported to show higher hardness with increasing Fe volume fraction [31]. The lowest microhardness values can be observed in the HAZ of Cu, around 77 HK, most likely due to the softening effect of grain growth, which is in agreement with the results of Chen et al. [33]. A relatively higher value of microhardness was observed in the HAZ of mild steel compared to the original microhardness of parent mild steel. Iqbal et al. [9] have reported similar results illustrating higher hardness in the HAZ of steel compared to parent material. They reported the formation of martensitic microstructure in the HAZ of mild steel due to rapid cooling during laser welding which is responsible for its relatively higher hardness. The variation in the average microhardness of weld nugget, HAZ of Cu, and HAZ of mild steel for samples produced using laser power from 1.1 kW to 1.5 kW is presented in Fig. 10. The average hardness inside the weld nugget was found to increase systematically with laser power, and a maximum value of 185 HK can be observed for the 1.5 kW sample. Again, this was expected due to the increased mixing of Cu and Fe inside the weld nugget with increasing heat input. On the other hand, the microhardness in the HAZ of Cu decreased with increasing laser power, illustrating a minimum value of 70 HK for the

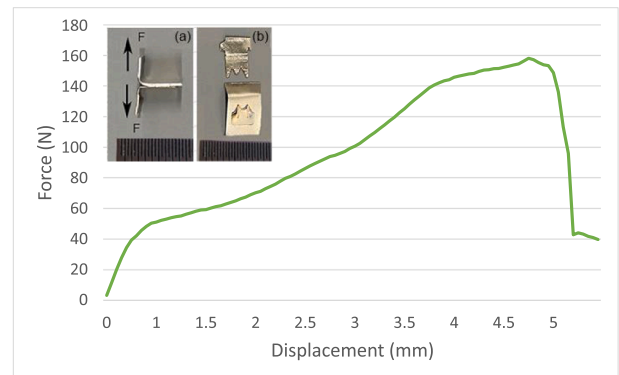


Fig. 11. The force–displacement curve of the 1.2 kW sample. (a) weld sample prepared for peel test (b) fractured sample after peel test showing fracture in HAZ of Cu.

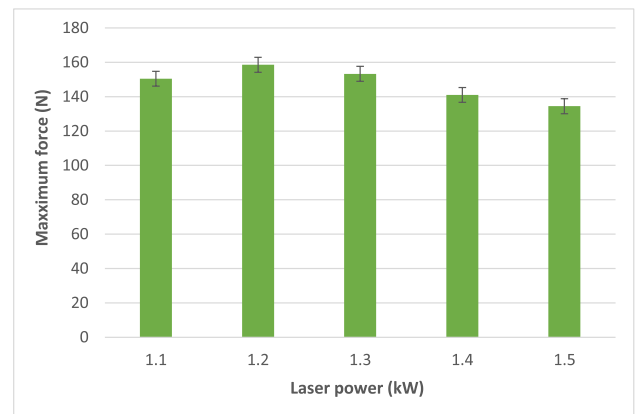


Fig 12. The maximum peel strength of weld samples for laser power from 1.1 kW to 1.5 kW.

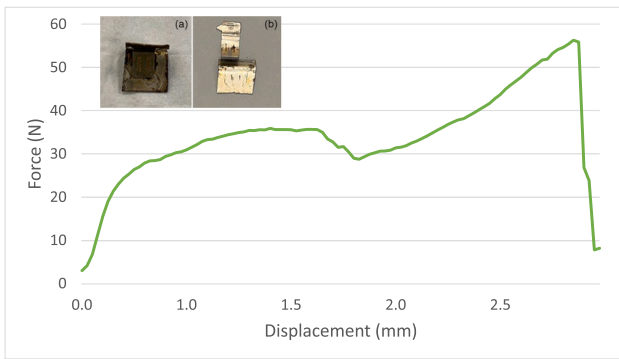


Fig. 13. The force–displacement curve for 1.2 kW corroded sample (a) weld sample after exposure to the corrosive environment for 144 h and before the peel test (b) fractured sample after the peel test showing interfacial failure.

1.5 kW sample. This can be attributed to increasing grain growth with higher laser powers. HAZ of mild steel experienced a slight increase that might be due to the formation of larger amounts of martensite due to higher heat input.

To investigate the effect of laser power on the joint strength, peel tests were performed on the weld samples. A typical force–displacement curve for the 1.2 kW sample along with images of the weld specimen before and after the peel test are shown in Fig. 11. A close view of the fractured specimen showed that the failure occurred outside the weld nugget and in the HAZ of Cu. This is quite in agreement with the lowest

microhardness values observed in this region. The peel strength was highest for this sample and measured to be 158.8 N. Fig. 12 shows the maximum peel strength of weld samples versus laser power. For the lowest laser power (1.1 kW), the interface width was relatively small and the peel strength was observed to be 147 N. The highest value of peel strength (158.8 N) was achieved for the 1.2 kW sample as the interface width and penetration depth increased. Similar results have been reported by Ventrella et al. [33] for laser welding of thin 316L stainless steel sheets. They reported that lap shear strength increased with penetration depth due to an increase in pulse energy. However, the current study showed that for higher laser powers (1.4 kW and above), excessive heat reduced the hardness in the HAZ of Cu, potentially by the grain growth, leading to material softness and consequently reduced the peel strength to 135 N for the 1.5 kW sample. The results indicated that the microstructural variations in the HAZ of Cu determined the weld strength. Therefore, the optimal welding conditions included partial weld penetration and sufficient interface width, without severe grain growth in the HAZ of Cu.

The weld samples were also peel tested after exposure to a Cl-rich corrosion environment for 144 h to see the effect of a corrosive environment on the joint strength. Fig. 13 shows the force–displacement curve and the top view of the 1.2 kW weld sample after being exposed to the Cl-rich environment, as well as the fractured specimen after peel testing. The effects of the corrosive attack can be seen on the surface of the welded sample. It was observed that the 1.2 kW sample experienced a massive drop in weld strength. The fractured specimen clearly showed that the failure occurred at the weld interface between the two sheets

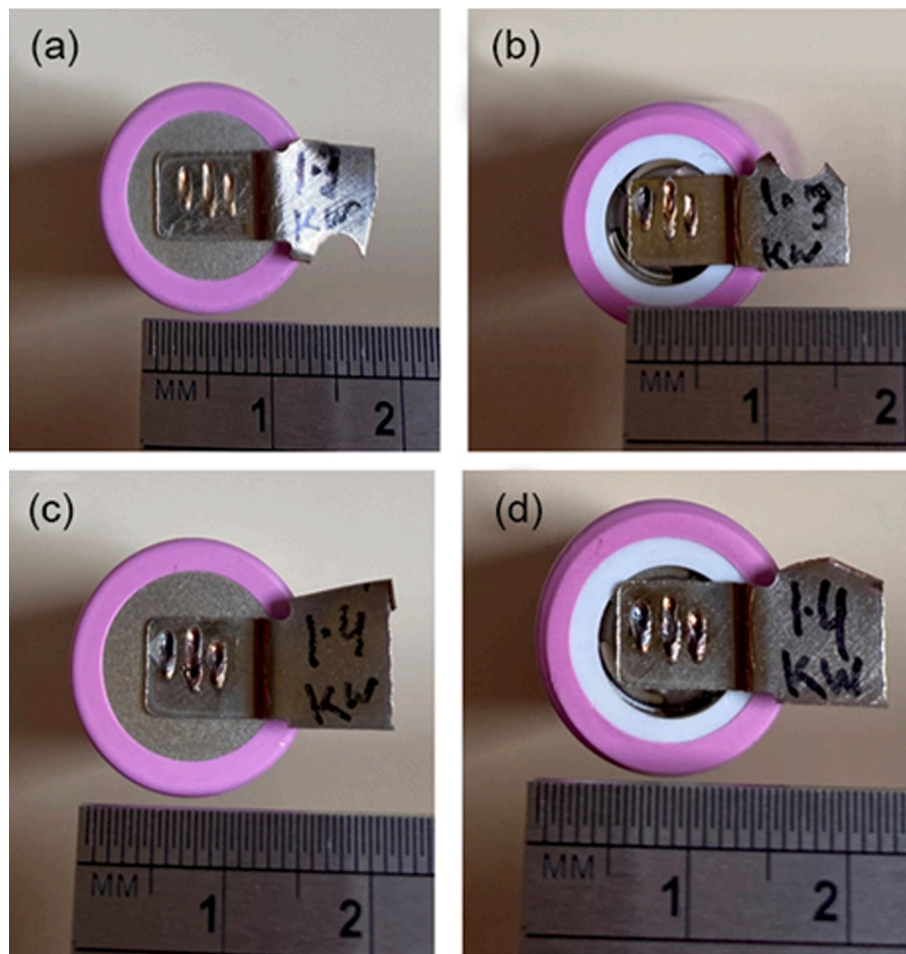


Fig. 14. The top view of the Ni-coated copper to cylindrical cell samples with the laser power of (a) 1.3 kW-negative terminal (b) 1.3 kW- positive terminal (c) 1.4 kW-negative terminal and (d) 1.4 kW-positive terminal.

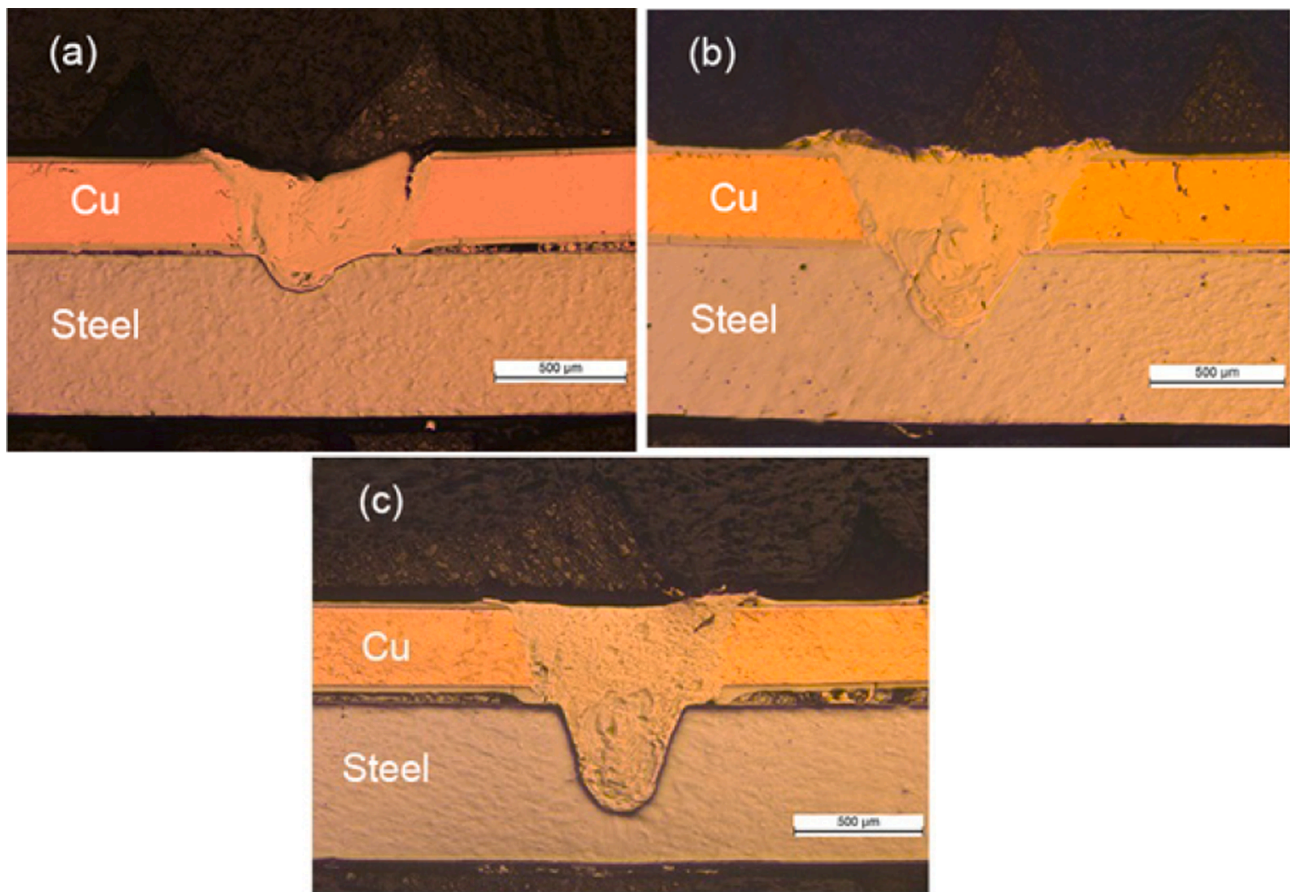


Fig. 15. The optical micrographs of Ni-coated copper to positive terminal weld samples for the laser power of (a) 1.3 kW (b) 1.4 kW and (c) 1.5 kW.

while the un-corroded sample fractured in the HAZ of Cu (Fig. 11). The maximum force was around 57 N, almost one-third of the un-corroded sample. Furthermore, the elongation was significantly reduced. The close examination of the fractured interface exhibited slight pitting, as shown in Fig. 13 b. As previously mentioned, during laser welding, the Ni coatings on Cu and mild steel were dissolved from the top of the weld region and the HAZ. This created a weak point where a corrosive solution could potentially penetrate and attack the weld region. Further in-depth investigations are required to quantify the corrosion performance of these dissimilar welds.

3.2. Cylindrical cell welding

The laser powers of 1.3 kW, 1.4 kW, and 1.5 kW were selected to weld Ni-coated copper to positive and negative terminals of commercially available 18650-type cylindrical cells made of Ni-coated mild steel. The rest of the process parameters were the same as used during the coupon welding. The exact grade and composition of cell terminals are not known, however positive and negative terminals had a thickness of 0.6 mm and 0.3 mm, respectively. The cell's internal structure showed that the positive terminal had a clear gap underneath; indicating that no direct heat sink was present during welding [34]. However, the bottom

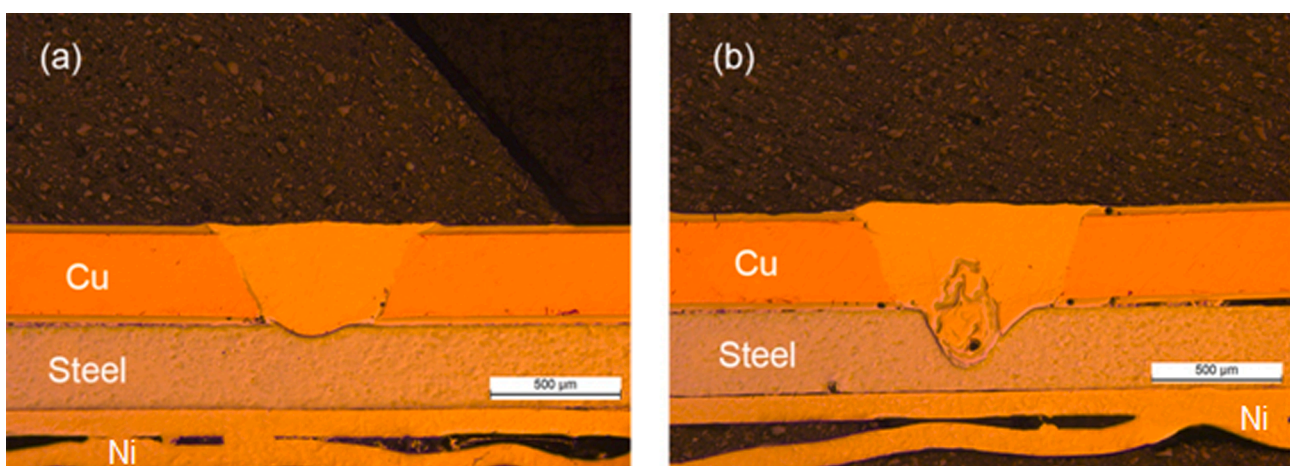


Fig. 16. The optical micrographs of Ni-coated copper to negative terminal weld samples for the laser power of (a) 1.3 kW and (b) 1.4 kW.

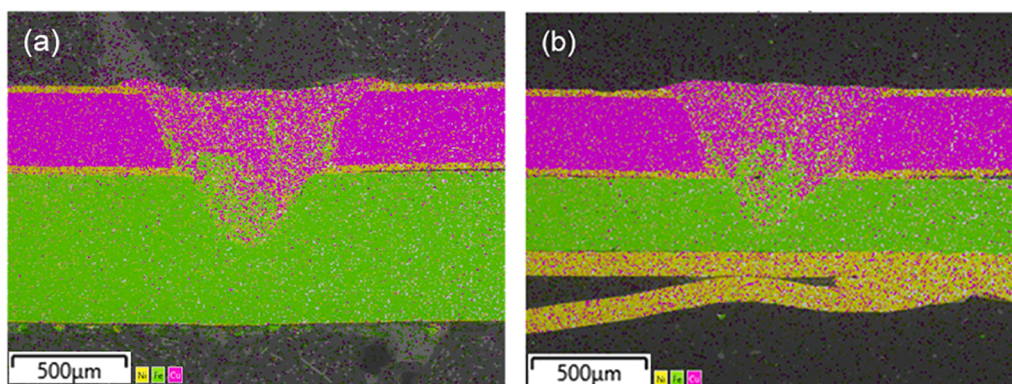


Fig. 17. The EDX images showing the elemental distribution of Ni, Cu, and Fe in (a) bus-bar to cell positive tab weld and (b) bus-bar to cell negative tab weld for the laser power of 1.4 kW.

of the negative terminals was connected to the inside of the cylindrical cell with a Ni strip which could act as a heat sink during welding. The top view of laser-welded busbar sections to positive and negative tabs for laser powers of 1.3 kW and 1.4 kW are shown in Fig. 14. The visual inspection of welds illustrated the formation of different weld bead surfaces for positive and negative terminals under the same process parameters. The difference in tab thickness and heat sink significantly influenced the melt pool temperature and melt flow, causing underfill and voids during welding. The number of voids formed was higher and the weld bead was more unstable in positive tabs as significant heat was retained inside the melt pool due to the absence of a heat sink. Furthermore, for higher laser power of 1.4 kW, visual inspection revealed an increase in the width of the weld bead and the number of weld defects due to an increase in the heat input. Some scattering of liquid metal is also evident in cylindrical samples, potentially due to the pressure exerted by the shielding gas during welding. The shielding gas was directed at the melt pool and delivered using copper tubing of 8 mm diameter. Such gas flow can cause turbulence in an excessively heated melt pool resulting in a scatter of liquid matter. The appropriate nozzle design for shielding gas flow can help avoid such scattering. Also reducing melt pool temperature through process refinement can further help to reduce the liquid matter scatter.

The optical micrographs of Ni-coated copper welds to positive and negative terminals for different laser powers are shown in Fig. 15 and

Fig. 16, respectively. As expected, the results indicated increased weld penetration and width for higher laser powers for both positive and negative terminals. However, by comparing positive and negative terminals, the weld penetration appeared to be less for the same laser power in negative ones due to the different internal heat sinks of each terminal. As seen in Fig. 16, a Ni substrate is attached to the bottom of negative terminals and inside the cell structure. It appears that the heat generated inside the terminal was partially dissipated through this Ni substrate which reduced the melt pool temperature resulting in less weld penetration in negative terminals.

Due to the lower thickness of the negative terminal, higher welding powers than 1.4 kW can cause overpenetration and damage the internal structure of the battery. Thus 1.4 kW can be considered the upper limit of welding power for negative terminals.

EDX maps for welds between Ni-coated copper and positive and negative terminals with a laser power of 1.4 kW are presented in Fig. 17. It was observed that the pattern of molten metal flow changed significantly with laser power, triggering convective mixing inside the weld nugget for both positive and negative terminals. This is evidenced by the EDX images, as shown in Fig. 17. It was found that similar to coupon welding Cu and Fe redistributed inside the weld nugget and they were not homogeneously mixed over the entire melt pool. Two regions with very different elemental concentrations were formed. The top of the weld nugget was predominantly Cu, coming from the top sheet, but with

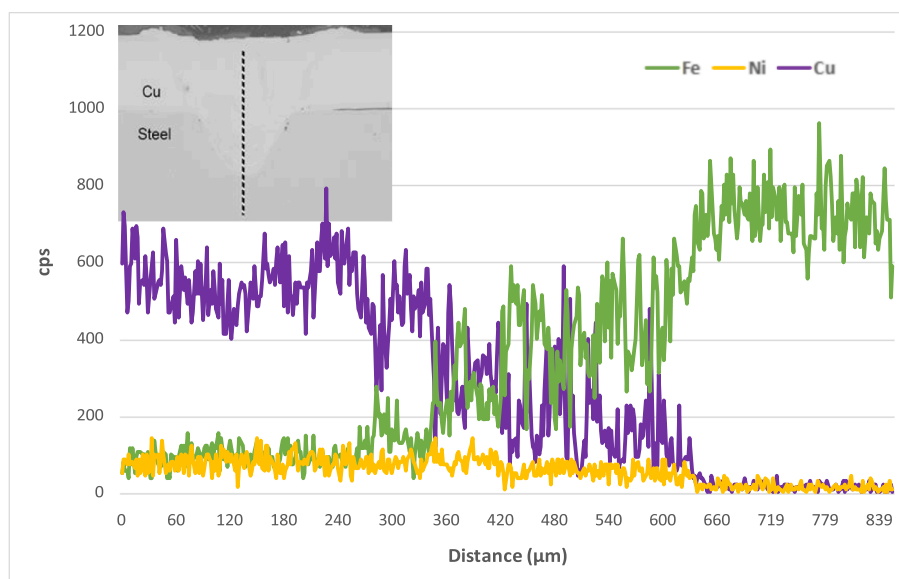


Fig. 18. The EDX line scan inside the weld nugget of bus-bar to positive tab weld (see insert) for laser power of 1.4 kW.

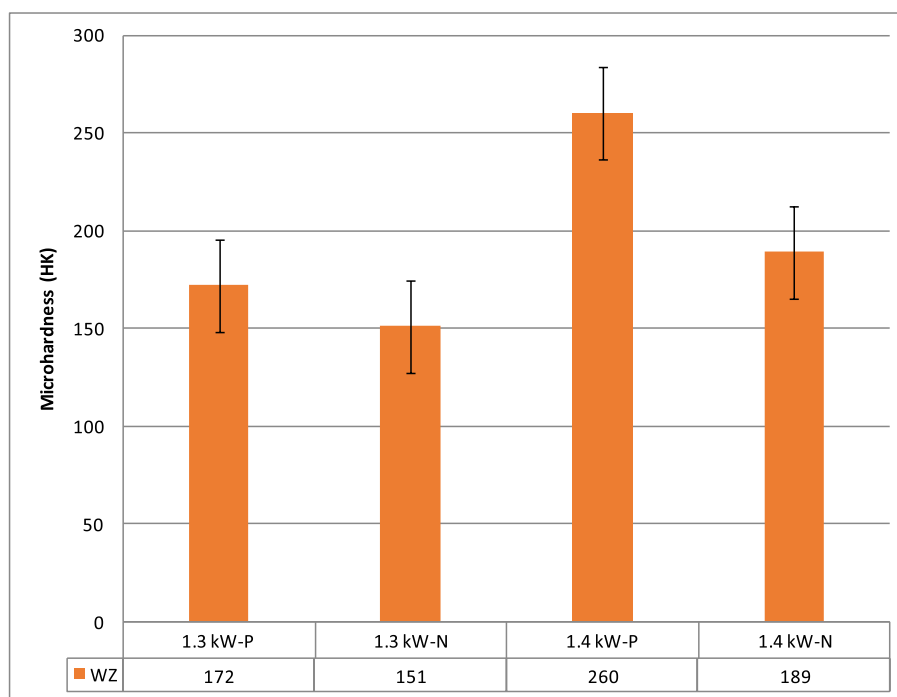


Fig. 19. The variation in average microhardness of weld zone (WZ) of Ni-coated copper to positive (P) and negative (N) terminal welds for the laser power of 1.3 kW and 1.4 kW.

a minor amount of Fe which flowed up from the cell terminal and was mixed with Cu. The bottom region was dominated by Fe, but a reasonable amount of Cu flowed down from the top Ni-coated copper. From Fig. 17, the phase separation between both elements is quite evident in this region. The EDX line scan for the positive terminal weld is shown in Fig. 18. As can be seen, the concentration of Fe, Cu, and Ni changed slowly in the top part of the weld nugget. However, Fe and Cu concentrations significantly fluctuate in the bottom region, representing the phase separation of Fe and Cu. The results from microstructural observation indicate that good quality welds with acceptable penetration and width can be achieved with a blue laser system however due to the presence of surface defects further process refinement is required.

The average microhardness of weld nuggets for positive and negative terminal welding with laser powers of 1.3 kW and 1.4 kW are shown in Fig. 19. As can be seen, the microhardness was always higher in positive terminal welding. This is because of excessive Cu and Fe mixing inside the weld nugget due to maximum heat retention in the absence of a heat sink which led to the presence of more Fe in the weld region. Furthermore, there is a direct relationship between microhardness and laser power. As the laser power increased, the microhardness also increased for both positive and negative terminal welding due to a larger weld pool and enhanced mixing of Fe and Cu elements.

4. Conclusions

The present study was focused on blue laser welding of low-thickness dissimilar materials namely Ni-coated Cu and mild steel for EV battery manufacturing. The effect of process parameters especially laser power on weld microstructure and mechanical performance of coupon samples and 18650-type cylindrical cells was investigated. The key observations of this study can be summarized as follows:

- Blue wavelength lasers offer a high-speed welding process for low thickness copper and steel for joining cylindrical cells in the EV battery pack. Due to the high absorption of blue wavelength laser in copper, conduction mode welding can be achieved for a range of laser powers.

- The laser weld width and penetration correlated with the laser power and with the increase in laser power a larger melt pool was created. In all samples, the weld width was always larger than the depth of penetration. With optimized laser power, welds with reasonable strength and surface quality can be produced. Lower laser power resulted in a lack of penetration while excessive laser power produced cracking and underfill.
- The weld nugget was generally heterogeneous in composition. The microstructural heterogeneity increased with laser power owing to convective mixing of Cu and Fe, forming Cu-Fe composite microstructure which significantly increased the microhardness inside the weld nugget compared to parent materials.
- The HAZ of copper was identified as the weak point during peel testing and fracture always occurred in this region due to potential softening induced by the grain growth.
- When exposed to a chloride-rich corrosion environment, The peel strength drastically decreased and the failure mode changed to interface fracture due to the pitting corrosion.
- The coupon welding provided an optimum window of process parameters, however further process refinement is needed when welding the Ni-coated copper to positive and negative cell tabs due to the different thicknesses of terminals and heat sinks associated with each of them.

CRediT authorship contribution statement

Amirhossein Sadeghian: Methodology, Investigation, Data curation, Writing – original draft, Visualization. **Naveed Iqbal:** Conceptualization, Methodology, Supervision, Writing – review & editing.

Declaration of Competing Interest

The authors declare that they have no known competing financial interests or personal relationships that could have appeared to influence the work reported in this paper.

References

- [1] S. Wang, M. Ge, Everything you need to know about the fastest-growing source of global emissions, *Transport* (2019).
- [2] S. Khalili, et al., Global transportation demand development with impacts on the energy demand and greenhouse gas emissions in a climate-constrained world, *Energies* 12 (20) (2019) 3870.
- [3] P.G. Pereirinha, et al., Main trends and challenges in road transportation electrification, *Transp. Res. Procedia* 33 (2018) 235–242.
- [4] W. Cai, Lithium-ion battery manufacturing for electric vehicles: a contemporary overview, *Adv. Battery. Manuf. Service. Manage. Syst.* 1 (2016).
- [5] A. Sadeghian, N. Iqbal, A review on dissimilar laser welding of steel-copper, steel-aluminum, aluminum-copper, and steel-nickel for electric vehicle battery manufacturing, *Opt. Laser. Technol.* 146 (2022), 107595.
- [6] A. Das, et al., Weldability and shear strength feasibility study for automotive electric vehicle battery tab interconnects, *J. Braz. Soc. Mech. Sci. Eng.* 41 (1) (2019) 54.
- [7] M.J. Brand, et al., Welding techniques for battery cells and resulting electrical contact resistances, *J. Storage. Mater.* 1 (2015) 7–14.
- [8] A. Das, et al., Joining technologies for automotive battery systems manufacturing, *World. Electric. Vehicle. J.* 9 (2) (2018) 22.
- [9] M.F.R. Zwicker, et al., Automotive battery pack manufacturing—a review of battery to tab joining, *J. Adv. Joining Process.* 1 (2020), 100017.
- [10] N. Iqbal, et al., Parametric Study of Pulse Arc Welding (PAW) and Laser Beam Welding (LBW) Techniques for Electrical Vehicle Battery Cells, *Trans Tech Publ.*, 2021.
- [11] N. Kumar, I. Masters, A. Das, In-depth evaluation of laser-welded similar and dissimilar material tab-to-busbar electrical interconnects for electric vehicle battery pack, *J. Manuf. Processes* 70 (2021) 78–96.
- [12] F. Lerra, A. Ascari, A. Fortunato, The influence of laser pulse shape and separation distance on dissimilar welding of Al and Cu films, *J. Manuf. Processes* 45 (2019) 331–339.
- [13] B. Mehlmann, et al., Spatially Modulated Laser Beam Micro Welding of CuSn6 and Nickel-plated DC04 Steel for Battery Applications, *J. Laser. Micro/Nanoeng* 9 (3) (2014).
- [14] U.F. Shaikh, et al., Electro-Thermo-Mechanical Behaviours of Laser Joints for Electric Vehicle Battery Interconnects, *IEEE*, 2019.
- [15] H.-C. Chen, et al., Enhanced welding efficiency in laser welding of highly reflective pure copper, *J. Mater. Process. Technol.* 216 (2015) 287–293.
- [16] M. Haubold, et al., Laser welding of copper using a high power disc laser at green wavelength, *Procedia CIRP* 74 (2018) 446–449.
- [17] S. Pricking, et al., High-power CW and long-pulse lasers in the green wavelength regime for copper welding, *International Society for Optics and Photonics*, 2016.
- [18] H. Wang, et al., Development of a high-power blue laser (445 nm) for material processing, *Opt. Lett* 42 (12) (2017) 2251–2254.
- [19] S.W. Britten, et al., Blue high-power laser sources for processing solutions in e-mobility and beyond, *Procedia. CIRP* 94 (2020) 592–595.
- [20] S. Katayama, *Fundamentals and details of laser welding*, Springer, 2020.
- [21] J.P. Davim, *Nontraditional machining processes, Manufacturing process Selection Handbook*, p. 205–226, 2013.
- [22] R. Indhu, et al., Overview of laser absorptivity measurement techniques for material processing, *Lasers Manuf. Mater. Process.* 5 (4) (2018) 458–481.
- [23] M.S. Zediker, et al., Laser welding components for electric vehicles with a high-power blue laser system, *J. Laser. Appl.* 32 (2) (2020), 022038.
- [24] K. Morimoto, et al., Bead-on-plate welding of pure copper sheet with 200 W high intensity blue diode laser, *International Society for Optics and Photonics*, 2020.
- [25] A. Das, et al., Blue laser welding of multi-layered AISI 316L stainless steel micro-foils, *Opt. Laser. Technol* 132 (2020), 106498.
- [26] M. Hummel, et al., New approaches on laser micro welding of copper by using a laser beam source with a wavelength of 450 nm, *J. Adv. Joining Processes* 1 (2020), 100012.
- [27] M.R. Pakmanesh, M. Shamanian, Optimization of pulsed laser welding process parameters in order to attain minimum underfill and undercut defects in thin 316L stainless steel foils, *Opt. Laser. Technol.* 99 (2018) 30–38.
- [28] M. Pastor, et al., Porosity, underfill and magnesium lose during continuous wave Nd: YAG laser welding of thin plates of aluminum alloys 5182 and 5754, *Weld. J.-New York*- 78 (1999) p. 207-s.
- [29] J. Zhou, H.L. Tsai, Porosity formation and prevention in pulsed laser welding, *J. Heat. Transfer* 129 (8) (2007) 1014–1024.
- [30] T. Suga, et al., Laser brazing of a dissimilar joint of austenitic stainless steel and pure copper, *Weld. Int* 30 (3) (2016) 166–174.
- [31] H. Sabetghadam, A.Z. Hanzaki, A. Araee, Diffusion bonding of 410 stainless steel to copper using a nickel interlayer, *Mater. Charact.* 61 (6) (2010) 626–634.
- [32] M. Velu, S. Bhat, Metallurgical and mechanical examinations of steel-copper joints arc welded using bronze and nickel-base superalloy filler materials, *Mater. Des.* 47 (2013) 793–809.
- [33] S. Chen, et al., Microstructural characteristics of a stainless steel/copper dissimilar joint made by laser welding, *Metall. Mater. Trans. A* 44 (8) (2013) 3690–3696.